Structural Mechanism of Endosome Docking by the FYVE Domain

Tatiana Kutateladze* and Michael Overduin

The recruitment of trafficking and signaling proteins to membranes containing phosphatidylinositol 3-phosphate [PtdIns(3)P] is mediated by FYVE domains. Here, the solution structure of the FYVE domain of the early endosome antigen 1 protein (EEA1) in the free state was compared with the structures of the domain complexed with PtdIns(3)P and mixed micelles. The multistep binding mechanism involved nonspecific insertion of a hydrophobic loop into the lipid bilayer, positioning and activating the binding pocket. Ligation of PtdIns(3)P then induced a global structural change, drawing the protein termini over the bound phosphoinositide by extension of a hinge. Specific recognition of the 3-phosphate was determined indirectly and directly by two clusters of conserved arginines.

Phosphoinositide 3-kinases direct membrane trafficking and signaling by the regulated production of PtdIns(3)P, PtdIns(3,4)P_2, PtdIns(3,5)P_2, and PtdIns(3,4,5)P_3. The monophosphorylated product is the most abundant because of its universal and constitutive expression in eukaryotic cells [reviewed in (*1*)]. PtdIns(3)P is recognized by the FYVE domain (*2*–*4*), which is named for its identification in the Fab1p, YOTB, Vac1p, and EEA1 proteins (*5*). Mammalian EEA1 fuses endosomes and relies on its FYVE domain for specific localization to PtdIns(3)P-enriched membranes and for recruiting regulatory Rab5 (*6, 7*) and syntaxin proteins (*8, 9*). However, the mechanism of membrane docking by the FYVE domain remains unclear.

Crystal structures of the lipid-free FYVE domains of yeast Vps27p (*10*) and fruit fly Hrs (*11*) suggest different models for PtdIns(3)P recognition. To better understand the mechanism of endosome targeting, we solved the structures of the FYVE domain of human EEA1 in the PtdIns(3)P-bound and phospholipid-free states (*12*) (Table 1) and defined the interactions in the specific complex with PtdIns(3)P-enriched micelles, a nonspecific dodecylphosphocholine (DPC) micelle complex, and aspecific complexes with PtdIns(5)P and PtdIns.

The fold of the FYVE domain in the free state was similar to its fold when bound to phosphoinositides or micelles (Fig. 1). The antiparallel sheet formed by the β1 and β2 strands was the central structural element and played a crucial role in PtdIns(3)P binding. The second β sheet formed an elongated extension that packed against Phe^{1405} and Leu^{1408} in the COOH-terminal α helix. Two zinc-binding clusters lay beneath and structured the PtdIns(3)P binding site; the first cluster also anchored the exposed hydrophobic Phe^{1364}-Ser-Val-Thr-Val^{1368} loop and mobile NH_2-terminus.

PtdIns(3)P was bound through a network of electrostatic, hydrogen-bonding, and hydrophobic interactions. The binding pocket for the inositol head group was defined by basic clusters at either end of the β1 strand, one proximal (Arg^{1369} and Arg^{1370}) and the other distal (Arg^{1374} and Arg^{1399}) to the exposed hydrophobic loop. The PtdIns(3)P molecule inserted parallel to β1, as judged by nuclear Overhauser effects (NOEs) observed between the 4′ and 5′ positions of the inositol ring and Arg^{1370}, His^{1372}, and Ile^{1379} (Fig. 2). The 1- and 3-phosphates were ligated by the proximal Arg^{1369} HN^{ε} and Arg^{1370} HN^{η} groups and by the distal Arg^{1374} HN^{ε} and HN^{η} groups, respectively, as reflected by changes induced in their resonances (Fig. 3A). The arginine resonance perturbations were reciprocated by comparable changes in the ^{31}P chemical shifts of the 1- and 3-phosphate groups (Fig. 3, B and C). The electrostatic nature of the interaction was emphasized by the FYVE domain's surface potential, with the most acute chemical shift changes occurring in the side chains that line the basic concave surface centered about the β1 strand (Fig. 4, A and B).

Specificity for PtdIns(3)P involved indirect recognition. Within mammalian cells, FYVE domains select PtdIns(3)P over other phosphoinositides such as PtdIns(5)P, its structurally most similar biological com-

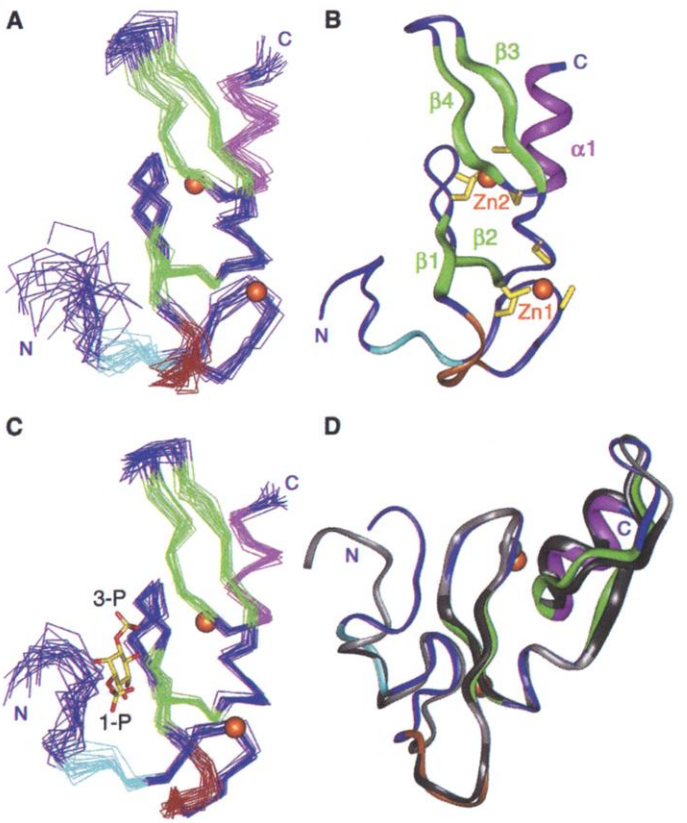

Fig. 1. Solution structures of the EEA1 FYVE domain. (**A**) The Cα traces of 20 structures are shown that comprise EEA1 residues 1346 to 1410 in the lipid-free form, with the β strands, helix, hinge, membrane insertion loop, and zinc ions colored green, magenta, cyan, brown, and orange, respectively. (**B**) Ribbon diagram of the structure closest to the average. The β1, β2, β3, and β4 strands and α1 helix consist of residues 1370 to 1372, 1379 to 1381, 1387 to 1391, 1396 to 1400, and 1402 to 1408, respectively. The two zinc ions (Zn1 and Zn2) are coordinated by eight cysteines whose side chains are shown in yellow. (**C**) The Cα traces of 20 PtdIns(3)P-bound structures are depicted as in (A). The PtdIns(3)P head group of the average structure is shown, with C and P atoms in yellow and O atoms in red. (**D**) Superposition of the PtdIns(3)P-bound and free structures, which are colored and gray, respectively. The view has been rotated slightly to reveal the structural differences.

Department of Pharmacology, University of Colorado Health Sciences Center, Denver, CO 80262, USA.

*To whom correspondence should be addressed. E-mail: tatiana.kutateladze@uchsc.edu

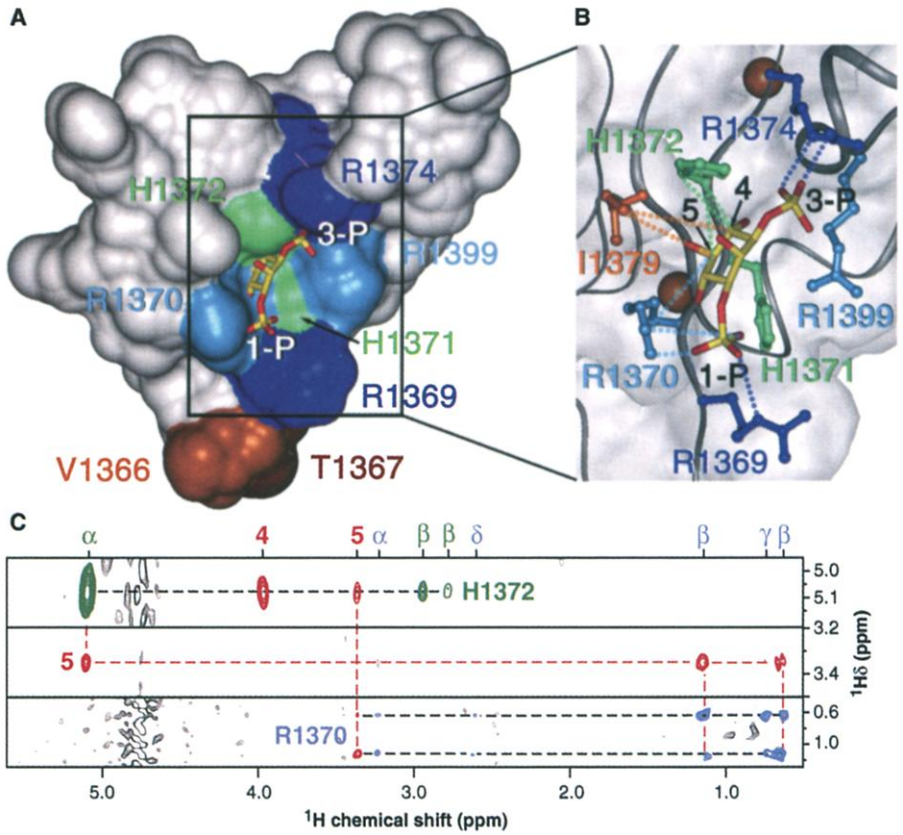

Fig. 2. Interactions in the PtdIns(3)P binding pocket. (**A**) The FYVE domain is shown as a solid surface with binding-site residues labeled and differentiated by color. PtdIns is shown as a stick model with C, O, and P atoms colored as in Fig. 1C. (**B**) The binding site is enlarged and depicted with a translucent surface. The protein backbone is shown as a gray ribbon. Binding-site residues are depicted as ball-and-stick models. The intermolecular NOEs and hydrogen bonds are indicated as dotted lines. (**C**) The His[1372] H^{α} and Arg[1370] H^{β}'s exhibit intermolecular NOE peaks (red) to the inositol ring 4- and 5-protons in the top and bottom panels, which are extracted from ^{13}C-edited NOE spectra. The intraresidue correlations of the His[1372] H^{α} and Arg[1370] H^{β} resonances are distinguished in green and blue, respectively. The middle panel depicts intermolecular ^{13}C filtered NOEs to the inositol ring 5-proton.

petitor. In fact, PtdIns(5)P did bind weakly to the EEA1 FYVE domain, inducing small but important chemical shift changes that paralleled the changes induced by PtdIns(3)P in the distal cluster (*13*). However, the arginine resonances in the proximal cluster were practically unaltered by PtdIns(5)P. Thus, we infer that the 5-phosphate could satisfy the distal cluster that normally ligates the 3-phosphate, whereas the 1-phosphate could not be accommodated by the proximal cluster. Consequently, specificity for PtdIns(3)P was determined indirectly by exclusion of the 1-phosphate of PtdIns(5)P, rather than by the inability of the 5-phosphate to mimic the 3-phosphate. Direct recognition of the 3-phosphate was also essential, because PtdIns, which lacks the 3-phosphate group, did not bind at all.

Global conformational changes were induced by PtdIns(3)P ligation. The 10 residues preceding the membrane insertion loop constituted the most disordered region of the unligated domain. However, upon interaction with PtdIns(3)P, this region became more constrained and moved toward the binding pocket (Fig. 1D). In particular, the NH_2-terminal Trp[1348] and Ala[1349] side chains exhibited new NOE contacts to binding-site residues including His[1372], Arg[1374], Gly[1377], Asn[1378], and Ile[1379]. This motion hinged on the Glu[1353]-Val-Gln[1355] residues, which became more extended in the complex, displaying large changes in their backbone resonances and dihedral angles. Moreover, a similar motion of this element was induced by PtdIns(5)P (*13*), suggesting that distal cluster occupancy was sufficient to engage the NH_2-terminus.

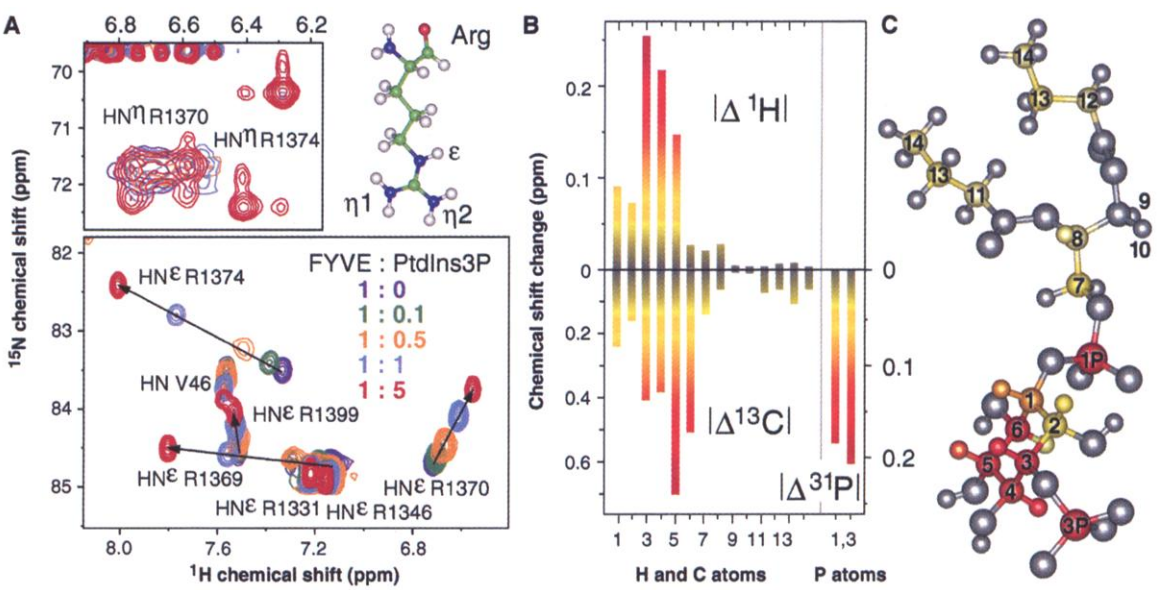

Fig. 3. Phosphate group recognition by arginines. (**A**) The H^{ε} resonances of Arg[1369] and Arg[1374] shift downfield upon PtdIns(3)P interaction (lower panel), indicating the formation of new hydrogen bonds. The H_2N^{η} resonances of the Arg[1370] and Arg[1374] become resolved only in the presence of PtdIns(3)P (upper panel), indicating that the guanidino group rotation is impeded by PtdIns(3)P coordination. Two regions of five ^{1}H-^{15}N correlation spectra of the FYVE domain (1 mM) with PtdIns(3)P concentrations of 0, 0.1, 0.5, 1, and 5 mM are superimposed. Arginine's structure is shown in the upper right. (**B**) PtdIns(3)P moieties recognized by the FYVE domain are indicated by absolute changes in the ^{1}H, ^{13}C, and ^{31}P chemical shifts of PtdIns(3)P induced by addition of equimolar FYVE domain. Atoms are numbered according to the positions indicated in (C). (**C**) Model of dibutanoyl PtdIns(3)P, with atom colors based on chemical shift perturbations induced by addition of equimolar FYVE domain, as indicated in (B).

The second β sheet also shifted closer to PtdIns(3)P, and as a result of tighter packing in the distal cluster, new NOEs appeared between Arg^{1374}, Arg^{1399} and neighboring residues near the basic cluster. Local rearrangements in the core were supported by chemical shift perturbations of buried residues, principally Ile^{1379} and Phe^{1380}. Together, these changes yielded a more globular structure in the FYVE domain complex.

Membrane insertion of an exposed hydrophobic loop stabilized the complex. Upon addition of micelles to the PtdIns(3)P-bound FYVE domain, the resonances of the Phe^{1364}-Ser-Val-Thr-Val^{1368} loop migrated and broadened (*13*), presumably because of direct insertion into the lipid bilayer (Fig. 4D). Indeed, membranes devoid of PtdIns(3)P can interact similarly with the FYVE domain, as judged by the small parallel shifts of the Val^{1366} and Thr^{1367} resonances upon addition of DPC alone (Fig. 4C). However, the nonspecific complex was much weaker because, even at a 600-fold excess concentration of DPC, the micelle-bound state was still not saturated (*13*). In addition, this nonspecific association was less extensive than the specific membrane interaction, which also involved Gln^{1355}, Phe^{1364}, Val^{1368}, Arg^{1369}, and Ala^{1382}. Membrane insertion critically enhances affinity, because the FYVE domain binds PtdIns(3)P-containing liposomes with a binding affinity of 50 nM (*14*) and binds micelle-free PtdIns(3)P with a micromolar affinity; furthermore, membrane localization of EEA1 is abrogated by Val^{1366}-Thr^{1367} mutations (*15*).

Nonspecific membrane insertion may position and prime the PtdIns(3)P binding site. The mobile Lys^{1347}-Trp-Ala^{1349} residues appeared to be pried away from the PtdIns(3)P pocket upon micelle association. In particular, the cross-peaks of these residues migrated in directions that were essentially exactly opposite to those induced by PtdIns(3)P ligation (*13*). Furthermore, pocket opening required articulation about the Asn^{1352}-Glu-Val^{1354} hinge. The backbone amide peaks of these hinge residues again shifted away from their closed conformation values. Thus, as a result of the mobility of the NH_2-terminal element and hinge, the FYVE domain existed in partially open, fully open, and closed conformations, depending on whether it was unligated, membrane-primed, or PtdIns(3)P-engaged. We postulate that sequential progression through these states allows FYVE domains to target to endosomal membranes in a rapid, specific, and stable fashion.

Although the structure of the EEA1 FYVE domain was similar in topology to those reported for Vps27p (*10*) and Hrs (*11*), the inferred binding mechanisms differ fundamentally. Direct ligation of the 3-phosphate by Arg^{220} of Vps27p (which is equivalent to Arg^{1399} of EEA1) is not substantiated by mutations (*14*) or nuclear magnetic resonance (NMR) data, which revealed distinct hydrogen bonding to Arg^{1374}. Ligation of the 1-phosphate by Hrs residues His^{178} and Arg^{208} (corresponding to EEA1 residues His^{1371} and Arg^{1399}, respectively) is inconsistent with the NMR studies, which instead implicated Arg^{1369} and Arg^{1370}. Lipid bilayer interactions predicted for the Vps27p Lys^{181}-Lys^{182} residues or the Hrs β3 and β4 strands were not observed in the homologous EEA1 residues. Moreover, the predicted membrane orientation of the Hrs FYVE domain differs from the micelle-binding interface of the EEA1 FYVE domain. Priming and clamping of the PtdIns(3)P pocket of EEA1 depended on a key tryptophan, which in the Hrs structure mediates dimerization. An irregular β strand in the crystal structures does not resemble any conformation of EEA1's flexible hinge and mobile element. Some of these differences may be influenced by unphysiological crystal contacts (*10*) and

Table 1. Experimental restraints and structural statistics.

Structural statistics	Free	Complex
Structure generation		
NOEs*		
Intermolecular	0	7
Intraresidue	161	162
Sequential	190	193
Medium-range	157	177
Long-range	223	285
Torsional restraints		
Phi	49	49
Psi	21	21
Hydrogen bond	13	18
Zinc	8	8
Average energies† (kcal mol^{-1})		
E_{total}	95.6 ± 4.6	109.9 ± 9.8
E_{NOE}	7.6 ± 2.3	15.4 ± 4.6
E_{bond}	2.6 ± 0.3	3.1 ± 0.6
E_{angle}	69.8 ± 1.7	74.2 ± 3.6
$E_{dihedral}$	0.24 ± 0.18	0.13 ± 0.11
$E_{improper}$	10.5 ± 0.5	10.5 ± 0.5
Restraint violations‡		
Average NOE violations per structure		
>0.27 Å	No violations	—
>0.34 Å	—	No violations
>0.20 Å	0.3	0.6
Average angle violations per structure (>2°)	0.35	0.05
Ramachandran analysis§ (residues 1357–1410/residues 1346–1410)		
Residues in most favored regions	83.1/75.9%	79.4/70.4%
Residues in additional allowed regions	16.6/21.5%	20.1/26.3%
Residues in generously allowed regions	0.3/2.1%	0.5/2.6%
Residues in disallowed regions	0/0.5%	0/0.7%
RMS deviations from ideal stereochemistry		
NOE (Å)	0.014 ± 0.002	0.019 ± 0.005
Bonds (Å)	0.0016 ± 0.000003	0.0018 ± 0.00007
Angles (°)	0.508 ± 0.004	0.524 ± 0.0006
Dihedral (°)	0.219 ± 0.134	0.157 ± 0.02
Impropers (°)	0.364 ± 0.01	0.365 ± 0.02
Coordinate precision (Å) (backbone/all heavy atoms)		
Secondary structure elements	0.52/1.07	0.43/0.93
Residues 1346–1410	1.25/1.87	0.52/0.99

*Medium-range NOEs are between residues separated by two to five residues; long-range NOEs are between residues separated by six or more residues. †Averaged energies of 20 structures with the lowest overall energies and fewest NOE violations. ‡Data for the intramolecular violations. §Prolines and glycines are not included. Analysis with AQUA and Procheck NMR (*20*).

dimerization interfaces seen in crystals (*11*) that are not supported by the apparent monomeric state of Hrs expressed in cells (*16*).

General 3-phosphoinositide recognition principles are shared by FYVE domains and pleckstrin homology domains (*17, 18*). Despite the lack of any homology, both domains ligate the 3-phosphate asymmetrically by HN^{ε} and HN^{η} groups of a conserved arginine, which is assisted by a second basic residue. Moreover, the 1-phosphate consistently forms hydrogen bonds with a polar residue separated from this arginine by three extended NH_2-terminal residues. Finally, an exposed hydrophobic loop proximal to the point of 1-phosphate ligation is positioned near the membrane.

In summary, we propose that EEA1 is targeted to endosomes through several stages. The FYVE domain is recruited to membranes through insertion of a conserved hydrophobic loop into the lipid bilayer. This weak membrane complex opens the binding site, priming it for specific recognition of PtdIns(3)P, ligation of which clamps the mobile termini down. Potential competitors such as PtdIns(5)P and PtdIns are excluded by indirect and direct readout of the phosphorylation state of the inositol ring. Simultaneous ligation of PtdIns(3)P and insertion into the membrane enhances affinity. Greater avidity for endosomes is afforded by parallel dimerization of EEA1's coiled-coil region (*19*). Finally, the structural plasticity of the FYVE domain suggests that it may play a key role in dynamically integrating Rab5 (*6, 7*) and syntaxins (*8, 9*) into the endosomal membrane fusion complex.

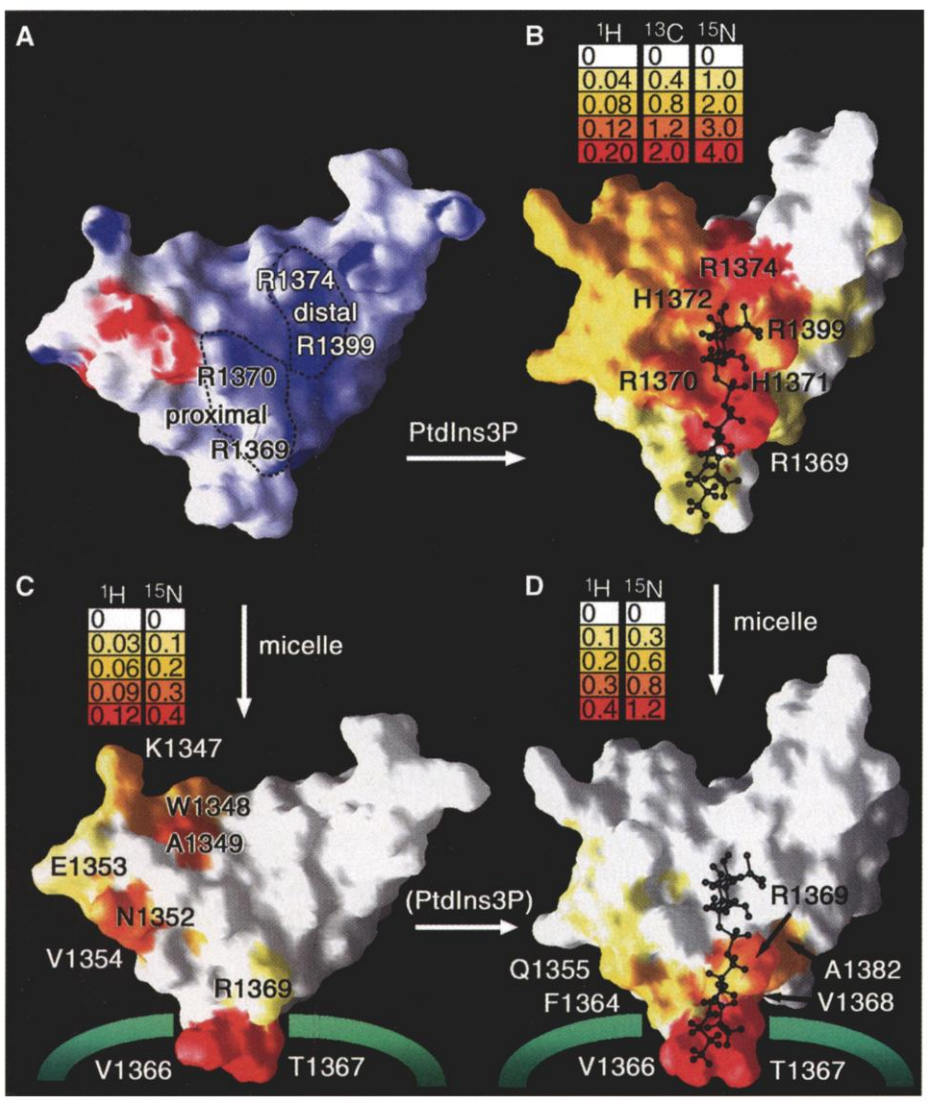

Fig. 4. Membrane docking mechanism. (**A**) The electrostatic surface potential of the lipid-free FYVE domain is colored blue and red for positive and negative charges, respectively, and is oriented as in Fig. 1D. (**B**) The PtdIns(3)P binding pocket is revealed by the surface of the complexed FYVE domain colored according to the extent of absolute chemical shift perturbations of ^{13}C, ^{15}N, and nonexchangeable ^{1}H's induced by addition of fivefold excess PtdIns(3)P; residues whose resonances show large, medium, small, very small, and negligible chemical shift differences are colored red, orange, deep yellow, light yellow, and white, respectively. (**C**) The site of nonspecific micelle association is shown by the surface of the PtdIns(3)P-free FYVE domain colored on the basis of absolute backbone amide chemical shift changes induced by addition of 600-fold excess DPC. The position of the lipid bilayer is shown in green. (**D**) The site of stable micelle association by the PtdIns(3)P-bound FYVE domain is pinpointed by the surface, which is colored according to the absolute backbone amide chemical shift changes induced by addition of 250-fold excess DPC to the PtdIns(3)P complex.

References and Notes

1. L. E. Rameh, L. C. Cantley, *J. Biol. Chem.* **274**, 8347 (1999).
2. C. G. Burd, S. D. Emr, *Mol. Cell* **2**, 157 (1998).
3. J. M. Gaullier *et al.*, *Nature* **394**, 432 (1998).
4. V. Patki, D. C. Lawe, S. Corvera, J. V. Virbasius, A. Chawla, *Nature* **394**, 433 (1998).
5. H. Stenmark, R. Aasland, B. H. Toh, A. D'Arrigo, *J. Biol. Chem.* **271**, 24048 (1996).
6. A. Simonsen *et al.*, *Nature* **394**, 494 (1998).
7. D. C. Lawe, V. Patki, R. Heller-Harrison, D. Lambright, S. Corvera, *J. Biol. Chem.* **275**, 3699 (2000).
8. H. M. McBride *et al.*, *Cell* **98**, 377 (1999).
9. A. Simonsen, J. M. Gaullier, A. D'Arrigo, H. Stenmark, *J. Biol. Chem.* **274**, 28857 (1999).
10. S. Misra, J. H. Hurley, *Cell* **97**, 657 (1999).
11. Y. Mao *et al.*, *Cell* **100**, 447 (2000).
12. Human EEA1 (residues 1325 to 1410) was expressed in *Escherichia coli* as a glutathione *S*-transferase fusion protein in unlabeled and uniformly ^{15}N- and $^{15}N/^{13}C$-labeled forms. Samples contained 0 to 2 mM of the FYVE domain, 10% or 99.9% $^{2}H_2O$, 20 mM tris-d_{11} buffer (pH 6.8 or 5.2), 200 mM KCl, 20 mM perdeuterated dithiothreitol, 1 mM NaN_3, 50 μM 4-amidinophenylmethane sulfonyl fluoride, 0 to 600 mM perdeuterated DPC, 0 to 5 mM dibutanoyl PtdIns(3)P, 0 to 1 mM PtdIns(5)P, and 0 to 0.6 mM PtdIns (Echelon Research Laboratories). NMR experiments were performed at 298 K on Varian INOVA (600 and 500 MHz) and Mercury (400 MHz) spectrometers. Resonances were assigned from homonuclear and ^{31}P-edited total correlation spectroscopy (TOCSY), ^{1}H-^{15}N heteronuclear single-quantum coherence (HSQC), ^{1}H-^{13}C HSQC, (HB)CBCA(CO)NNH, HNCACB, HNCO, HCCH, H(CCO)NH, and C(CO)NH TOCSY spectra. NOEs were assigned from ^{15}N- and ^{13}C-edited NOE spectroscopy (NOESY) and ^{13}C F_1-filtered, F_2-edited NOESY experiments. Spectra were processed with NMRPipe and in-house software programs (http://biomol.uchsc.edu). Structures were calculated using X-PLOR 3.84.
13. See *Science* Online (www.sciencemag.org/cgi/content/full/291/5509/1793/DC1).
14. J. M. Gaullier, E. Ronning, D. J. Gillooly, H. Stenmark, *J. Biol. Chem.* **275**, 24595 (2000).
15. T. G. Kutateladze *et al.*, *Mol. Cell* **3**, 805 (1999).
16. A. Hayakawa, N. Kitamura, *J. Biol. Chem.* **275**, 29636 (2000).
17. S. E. Lietzke *et al.*, *Mol. Cell* **6**, 385 (2000).
18. K. M. Ferguson *et al.*, *Mol. Cell* **6**, 373 (2000).
19. J. Callaghan, A. Simonsen, J. M. Gaullier, B. H. Toh, H. Stenmark, *Biochem. J.* **338**, 539 (1999).
20. R. A. Laskowski, J. A. Rullmann, M. W. MacArthur, R. Kaptein, J. M. Thornton, *J. Biomol. NMR* **8**, 477 (1996).

21. Supported by NIH grant CA85716, the American Cancer Society, the Pew Scholars Program, the University of Colorado Cancer Center, and the NMR facilities of the University of Colorado Health Sciences Center and the University of Denver. Structural data have been deposited in the Research Collaboratory for Structural Bioinformatics (RCSB) Protein Data Bank (1HYJ and 1HYI) and BioMagResBank (4579 and 4898). We thank T. de Beer, D. N. M. Jones, C. G. Burd, and S. D. Emr for comments, and L. E. Kay for pulse sequences.

5 December 2000; accepted 23 January 2001